Supporting Information

Triazole-Boosted Dual Structured Covalent Triazine Frameworks for Ultra-Stable High Energy and Power Density Aqueous Supercapacitor and Notable Selective CO_2 Capture

Section A. General information:

All chemical reagents were procured from reputable commercial sources and utilized as received unless specified otherwise. Anhydrous Zinc chloride (Alfa-Aesar) was stored in a vacuum desiccator and further dried at 110 °C under vacuum oven before implementation. The synthesis of 3,3′,5,5′-Tetraethynyl-2,2′,4,4′,6,6′-hexamethylbiphenyl and 4-azidocyanobenzene followed established literature procedures, commencing from 2-bromomesitylene and 4-aminobenzonitrile, respectively. Requisite materials such as 2-bromomesitylene, magnesium turnings, anhydrous $FeCl_3$, 1,2-dibromoethane, bis(triphenylphosphine)palladium(II) chloride, trimethylsilylacetylene, potassium carbonate, 4-aminobenzonitrile, sodium azide were sourced from Alfa-Aesar. Additionally, $HIO_4 \cdot 2H_2O$, iodine, copper(I) iodide, sodium thiosulphate, glacial acetic acid, and common organic solvents including dichloromethane, hexane, chloroform, and THF were procured from Spectrochem (India). THF and TEA were distilled from sodium/benzophenone and KOH, respectively, before application. All moisture-sensitive reactions were conducted under a nitrogen atmosphere within the Schlenk line using oven-dried glassware.

Section B. Experimental measurements:

Fourier-transform Infrared spectra (FT-IR) of monomer and as-synthesized CTF materials were obtained using a Perkin Elmer Spectrum-GX spectrophotometer with KBr pallet in transmittance mode with background corrected form. **High-resolution mass spectra** were recorded on a Bruker Micro TOF-QII mass spectrometer by electrospray ionization (ESI). **Powder X-ray diffraction (PXRD)** data were collected on a Rigaku Ultima-IV diffractometer using monochromated Cu-K_α (λ = 1.54060 Å) radiation with a scan speed of 2° min^{-1} and a step size of 0.01° in 2θ with an operating voltage of 40 kV and current of 30 mA of the X-ray tube. **Thermogravimetric analyses** were carried out using Netzsch STA 449F3-jupiter thermogravimetric-differential scanning calorimetry (TG-DSC) analyzer using an aluminium oxide crucible. Heating was performed from room temperature to 1000^{o}C under a nitrogen stream with a heating rate of 10 °C/min. **The Raman spectra** were carried out on a Horiba LabRAM HR confocal micro-Raman system with an excitation source of a 532 nm diode-pumped solid-state laser. **Field emission scanning electron microscopy (FE-SEM)** images were taken using Carl Zeiss AG Supra Gemini 55 at an accelerating voltage of 15 kV and equipped with OXFORD energy dispersive X-ray spectrometer. The powder samples were dispersed in dichloromethane and the suspension was drop casted on a clean piece of silicon wafer. **Transmission electron microscopy (TEM)** images were captured using a JEOL-JEM F 200 TEM operated at 200 kV. The powder samples were dispersed in ethanol and one drop of the suspension was drop cast on a carbon-coated copper grid. **Elemental analysis** (C, H,

and N) was performed on a Thermo Scientific Flash 2000 Organic Elemental Analyzer. **High-resolution X-ray photoelectron spectroscopy (XPS)** spectra were recorded with PHI 5000 Versa Probe II XPS with AES module comprising argon ion and C60 sputter guns. All **low-pressure gas adsorption-desorption experiments** (up to 1 bar) were carried out on Quantachrome Autosorb-iQ surface area & pore size analyser. Before gas adsorption experiment sample was degassed first at 140 ^{o}C under a dynamic vacuum for 12 hours. The N_2 (77 K) isotherm was measured using a liquid nitrogen bath. CO_2 and N_2 isotherms at 273 K, 298 K, and 308 K were measured using a jacketed recirculating dewar containing water and ethylene glycol (1:1 ratio) mixture, and the dewar was connected to a chiller (JULABO, FL300, working temperature range: -20 to +40^{o}C, temperature stability: ± 0.5^{o}C) having circulating methanol to precisely achieve targeted analysis temperature. ESPEC SH-222 Bench-top type Temperature & Humidity Chamber is used for temperature and humidity dependent electrochemical measurements. The Brunauer-Emmett-Teller (BET) surface area was calculated over the relative pressure range of 0.05 – 0.3 P/P_0. Total pore volumes were measured at a relative pressure near 0.99 P/P_0 while microporosity was estimated by measuring the pore volume at a relative pressure of 0.1 P/P_0. Pore size distributions and pore volumes were derived from the isotherms using the non-local density functional theory (NL-DFT) slit pore model on carbon.

Section C. Synthetic procedure:

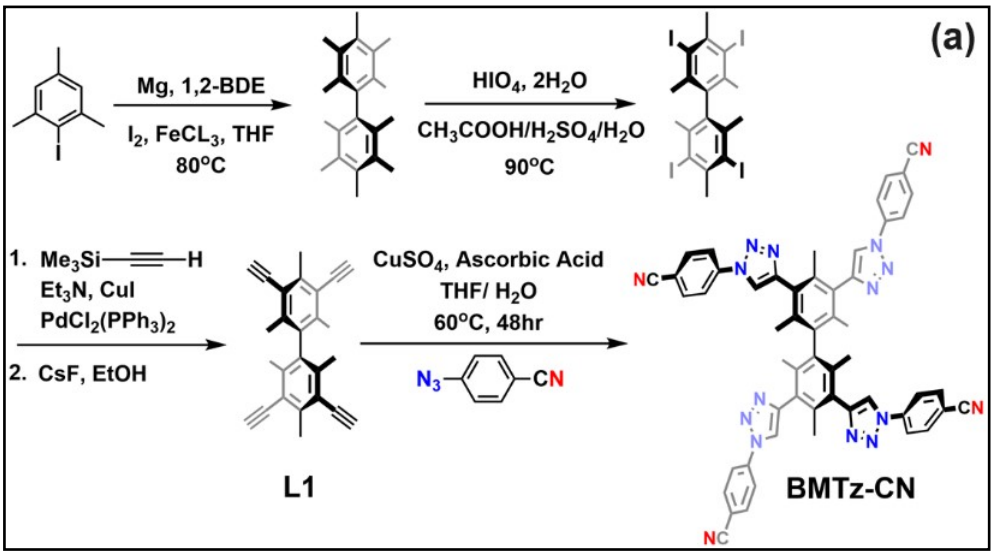

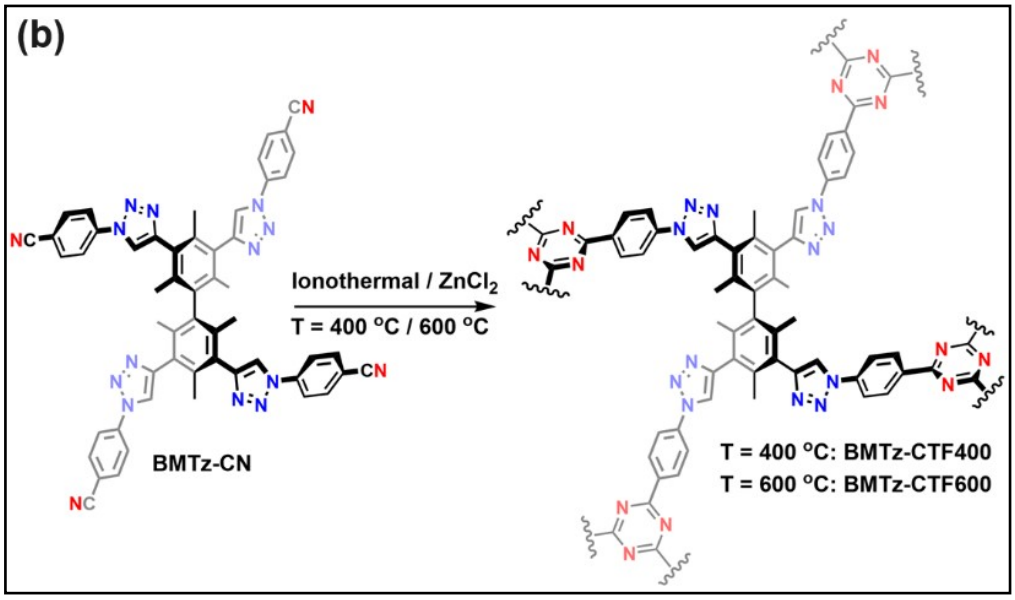

Scheme S1: (a) Detail synthetic route of BMTz-CN monomer. (b) Ionothermal synthetic process for BMTz-CTF materials

3,3′,5,5′-Tetraethynyl-2,2′,4,4′,6,6′-hexamethylbiphenyl (L1): It was synthesized according to described literature procedure with a good yield[S1], 70% over four steps. ^{1}H NMR (300MHz, $CDCl_3$) δ: 3.52 (s, 4H), 2.67 (s, 6H), 2.01 (s, 12H) ppm. ^{13}C NMR (xxx MHz, $CDCl_3$) δ: 143.03, 139.25, 137.17, 120.79, 85.54, 81.39, 20.09, 18.77 ppm.

3,3′,5,5′-Tetra-[4-(1-H-1,2,3-triazol-1-yl)benzonitrile]-2,2′,4,4′,6,6′-hexamethylbiphenyl (BMTz-CN): To a two-necked round-bottom flask charged with 3,3′,5,5′-Tetraethynyl-2,2′,4,4′,6,6′-hexamethylbiphenyl (0.40 g, 1.19 mmol) and 2.5:1 degassed mixture of tetrahydrofuran (60mL) and water (24 mL), 4-azidobenzonitrile (0.793 g, 5.50 mmol), $CuSO_4 \cdot 5H_2O$ (0.093 g, 0.373 mmol), and sodium ascorbate (0.148 g, 0.747 mmol) was added, under a nitrogen gas atmosphere. The contents were heated to 60°C under nitrogen for 2 days. After cooling down THF was removed in vacuo, and the reaction mixture was washed with 100 ml 2M EDTA solution and extracted with ethyl acetate three times. The combined organic extract was washed three times with distilled water. The organic phase was then dried over anhydrous Na_2SO_4, and the solvent was removed in vacuo to obtain the crude product. The latter was purified by silica gel column chromatography (25% ethyl acetate: 75% chloroform) to obtain **BMTz-CN** as an off-white solid powder. Yield = 0.960g (88%); FT-IR (KBr solid) cm^{-1} 3140, 3109, 2925, 2230, 1607, 1515, 1436, 1414, 1390, 1324, 1284; ^{1}H NMR (300MHz, $CDCl_3$) δ: 9.14 (s, 4H), 8.22 (d, 8H), 8.12 (d, 8H), 1.90 (s, 6H), 1.83 (s, 12H) ppm; ^{13}C NMR (100 MHz, DMSO-d_6) δ: 146.66, 140.04, 138.56, 136.95, 136.46, 134.82, 129.16, 123.09, 120.71, 118.62, 11.40, 19.38, 18.70 ppm.

Section D: ^{1}H and ^{13}C NMR spectroscopy analysis:

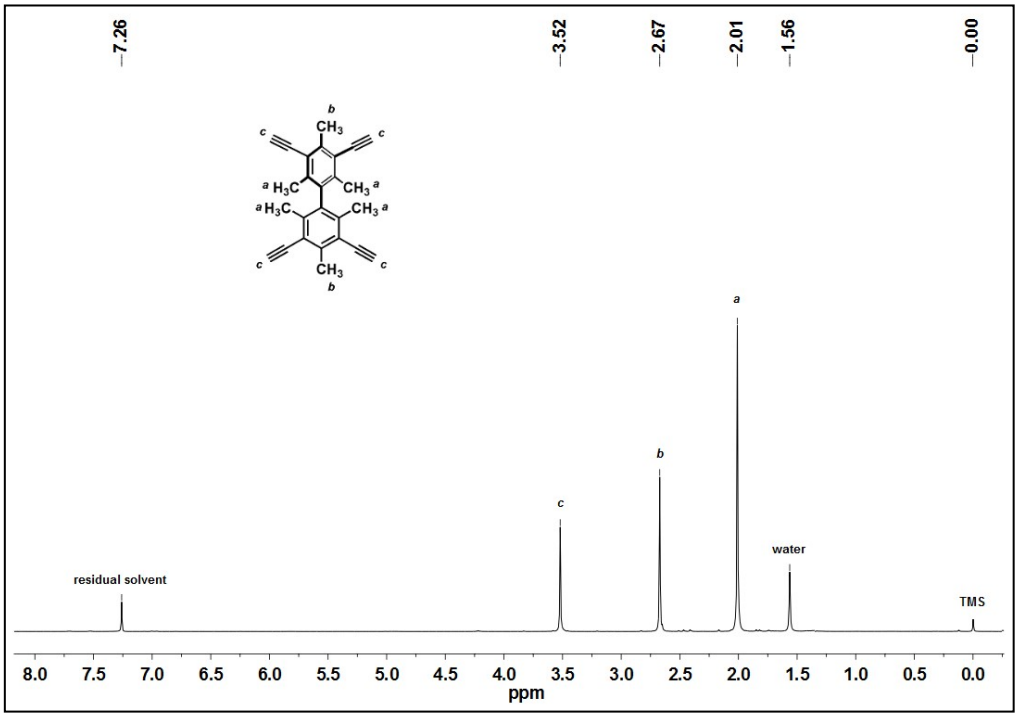

Figure S1: ^{1}H NMR spectra of 3,3',5,5'-tetraethynyl-2,2',4,4',6,6'-hexamethylbiphenyl

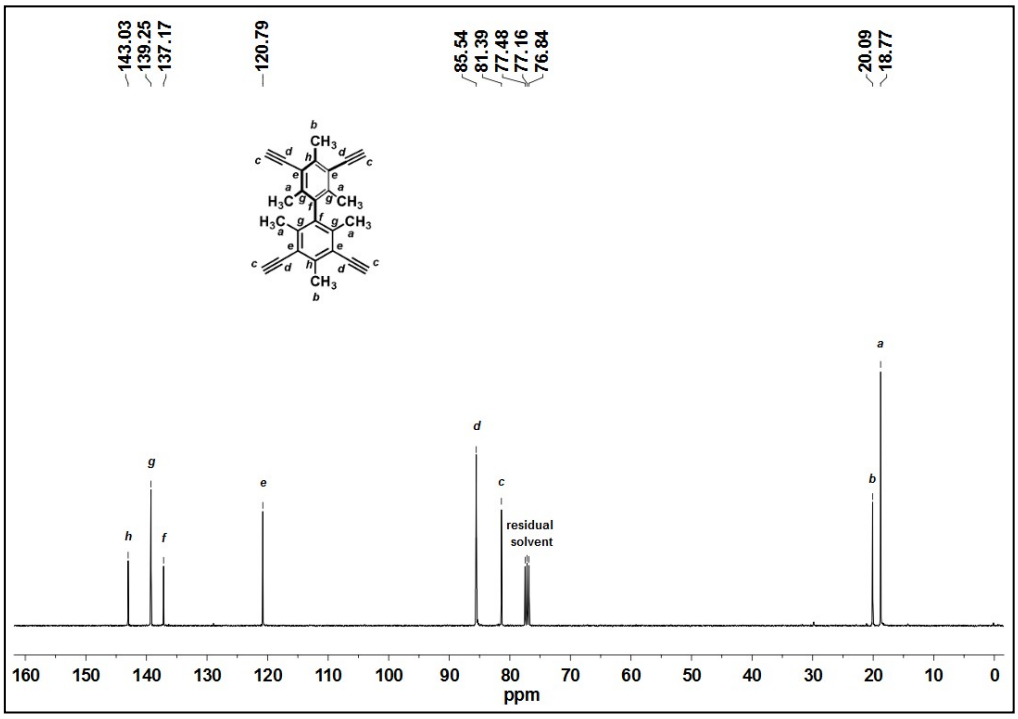

Figure S2: ^{13}C NMR spectra of 3,3',5,5'-tetraethynyl-2,2',4,4',6,6'-hexamethylbiphenyl

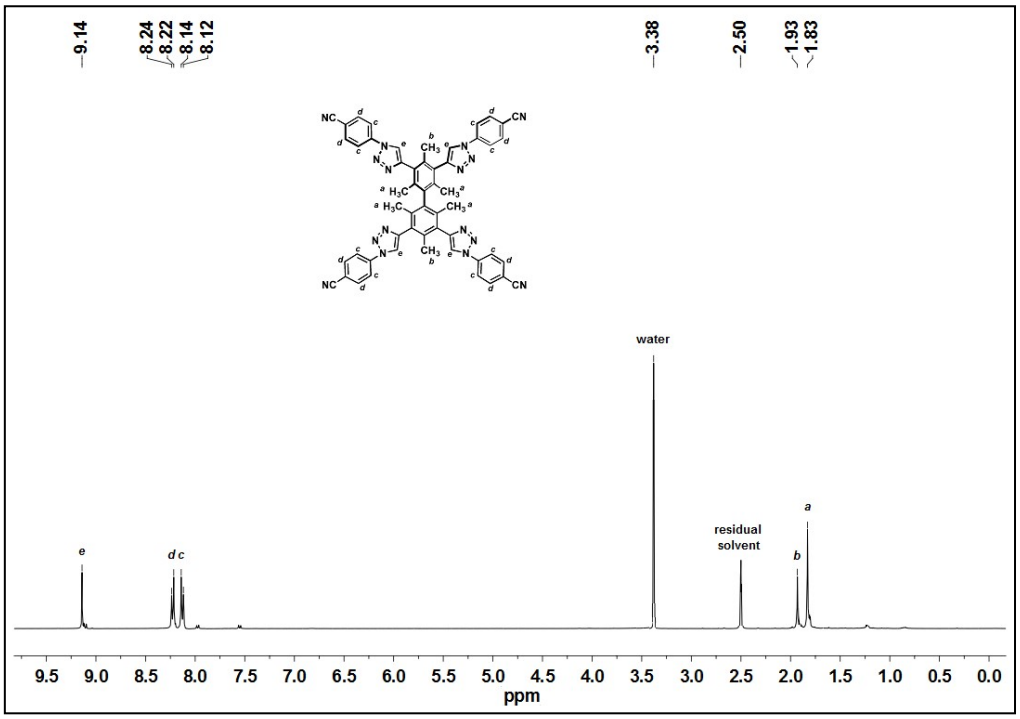

Figure S3: ^{1}H NMR spectra of 3,3′,5,5′-Tetra-[4-(1-H-1,2,3-triazol-1-yl)benzonitrile]-2,2′,4,4′,6,6′-hexamethylbiphenyl monomer (BMTz-CN)

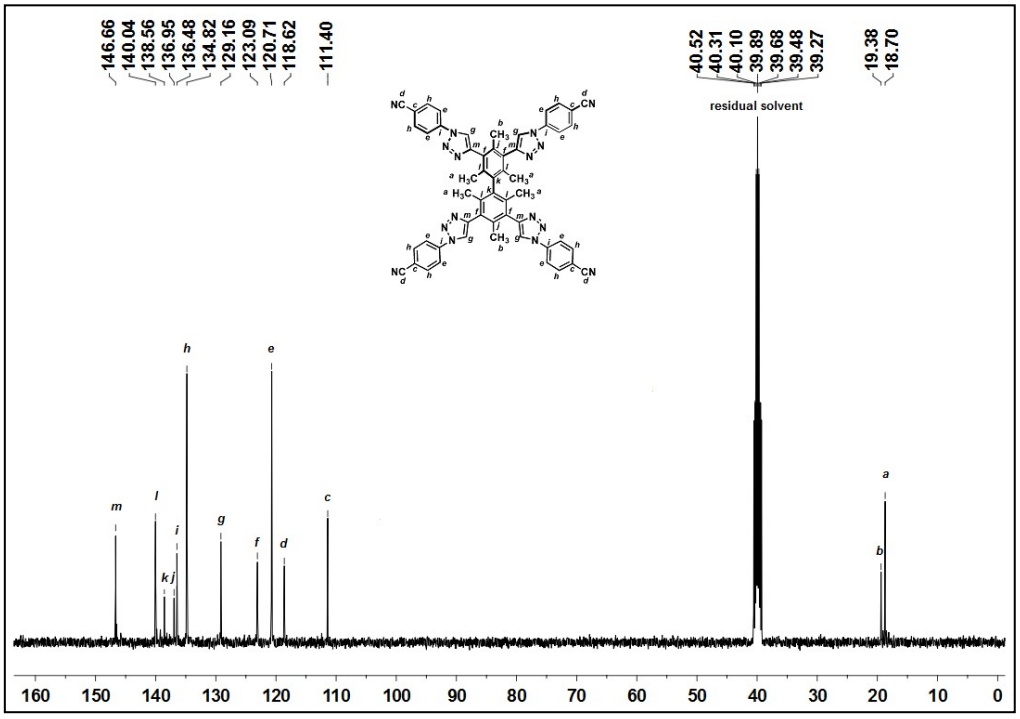

Figure S4: ^{13}C NMR spectra of 3,3′,5,5′-Tetra-[4-(1-H-1,2,3-triazol-1-yl)benzonitrile]-2,2′,4,4′,6,6′-hexamethylbiphenyl monomer (BMTz-CN)

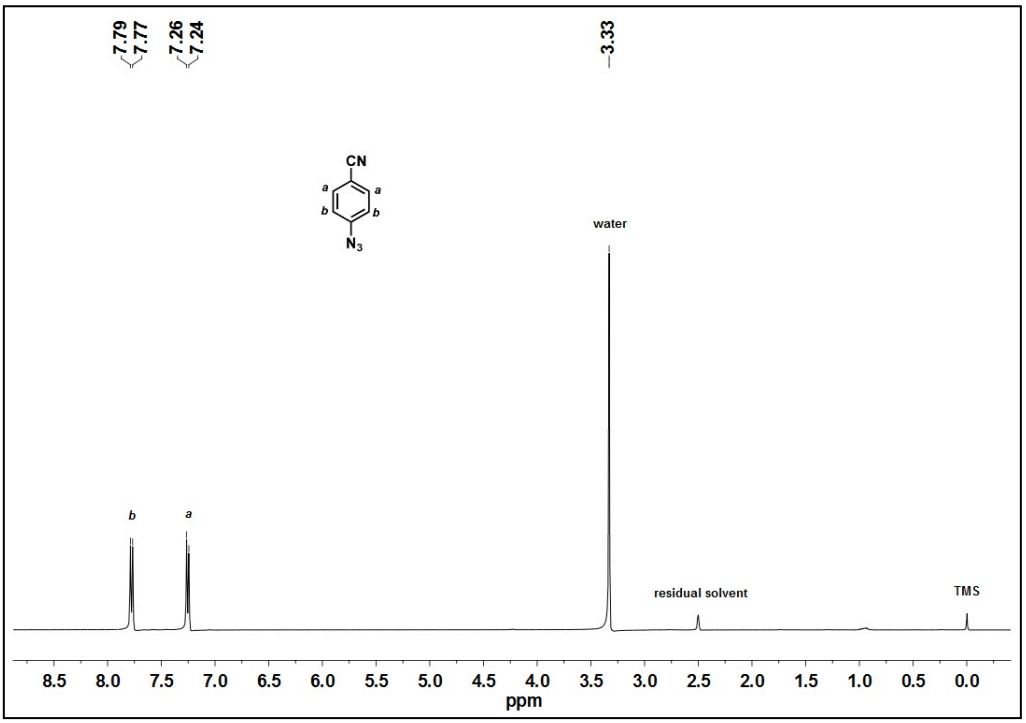

Figure S5: ^{1}H NMR of 4-azidobenzonitrile.

Section E: HR-MS (ESI) analysis of the monomer:

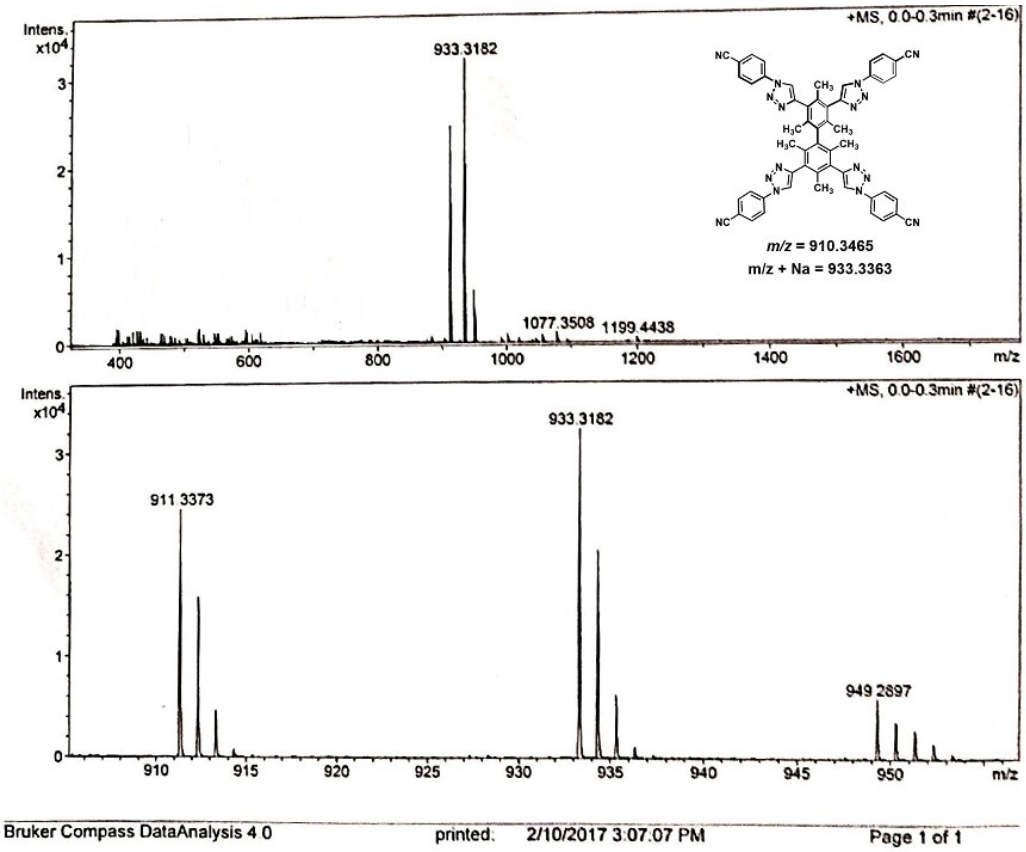

Figure S5: HR-MS (ESI) spectra of 3,3′,5,5′-Tetra-[4-(1-H-1,2,3-triazol-1-yl)benzonitrile]-2,2′,4,4′,6,6′-hexamethylbiphenyl monomer (**BMTz-CN**)

Section F. Elemental analysis:

Table S1. Elemental analysis of **BMTz-CTF** materials from the combustion process

Sample	Elemental Analysis (Calculated)			C/N	C/H
	C	N	H		
BMTz-CN	63.16	24.55	2.94	2.57	21.48
Sample	Elemental Analysis (Experimental)			C/N	C/H
	C	N	H		
BMTz-CTF400	62.10	8.61	2.38	7.21	26.09
BMTz-CTF600	60.88	7.19	2.05	8.46	29.69

Section G. XPS survey scan and CO_2 uptake at variable conditions:

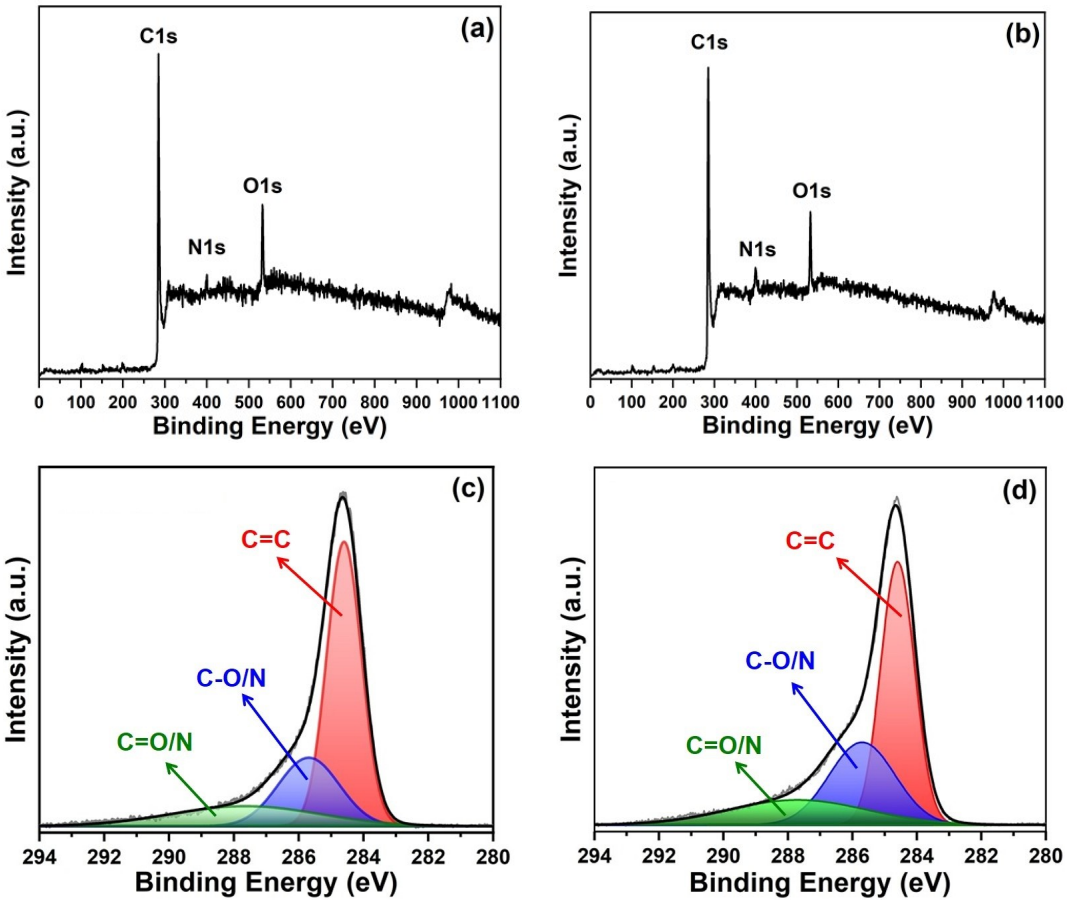

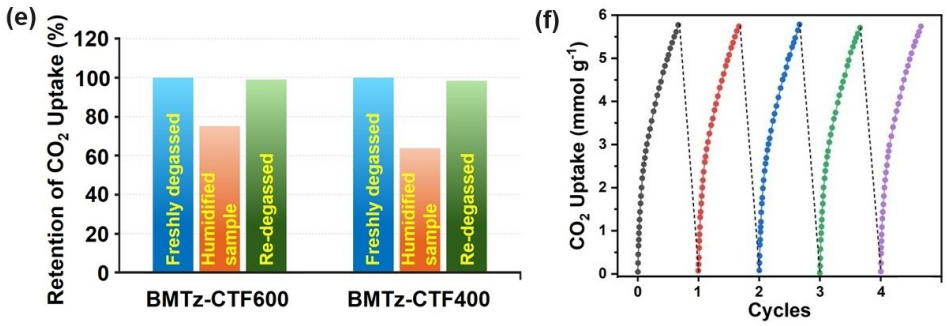

Figure S6: XPS survey spectra of (a) BMTz-CTF400 and (b) BMTz-CTF600. C1s deconvoluted XPS spectra of (c) BMTz-CTF400 and (d) BMTz-CTF600. (e) CO_2 uptake was measured at 298 K and 1 bar using humidified BMTz-CTF600 sample. (f) BMTz-CTF600 sample underwent four cycles of CO_2 uptake at 273 K and 1 bar.

Section H. Isosteric heat of adsorption:

The isosteric heat of adsorption, Q_{st}, defined as

$$Q_{st} = RT^2\left(\frac{\partial \ln p}{\partial T}\right)_q$$

were determined from the pure component CO_2 isotherm fits at 298 K and 273 K using the Clausius-Clapeyron equation.

Section I: Details procedure for IAST calculation:

To predict their selectivity toward a CO_2/N_2 binary mixture, ideal adsorbed solution theory (IAST) calculations using Henry's law, Langmuir, Dual-site Langmuir, and Brunauer-Emmett-Teller adsorption models were employed based on the single-component **BMTz-CTF400 and -CTF600** isotherms.[49] Figure S4 and S8 show the predicted CO_2/N_2 selectivity as a function of the pressure when the gas-phase mole fraction is 15/85, which is a typical feed composition of flue gas. The IAST selectivity toward CO_2 in the presence of N_2 at 308 K, 298 K, and 273 K and 1 bar are 65, 57, 29 for **BMTz-CTF400** and 71, 82, and 66 for **BMTz-CTF600**, respectively.

N_2: *Li(P)* for species I follows a Henry's Law isotherm with Henry's constant K_H and pressure P:

$$Li(P) = K_H P$$

CO_2: *Li(P)* for species I follows a Langmuir isotherm with saturation loading M and Langmuir constant Ki:

$$Li(P) = M\frac{KiP}{1 + KiP}$$

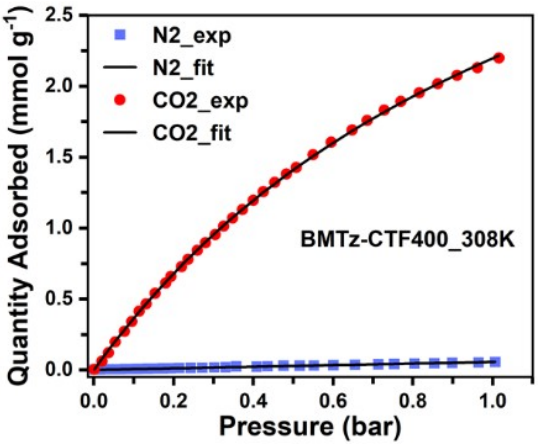

	K_H	M	Ki
CO_2		4.976480185	0.79026027
N_2	0.0565668960695302		

Figure S7. IAST fitting for CO_2 and N_2 isotherm measured at 308 K in **BMTz-CTF400**.

N_2: *L(P)* for species I follows a Henry's Law isotherm with Henry's constant K_H and pressure *P*:

$$L(P) = K_H P$$

CO_2: *L(P)* for species I follows a Langmuir isotherm with saturation loading *M* and Brunauer-Emmett-Teller (BET) constant *K*:

$$L(P) = M\frac{K_A P}{(1 - K_B P)(1 - K_B P + K_A P)}$$

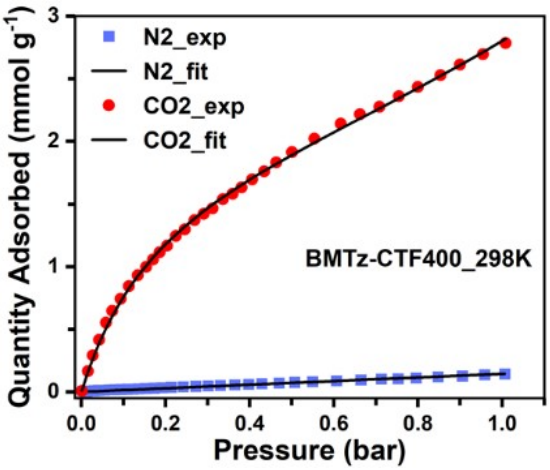

	K_H	M	K_A	K_B
CO_2		2.024212972	5.474238015	0.35365274
N_2	0.145017449138117			

Figure S8. IAST fitting for CO_2 and N_2 isotherm measured at 298 K in **BMTz-CTF400**.

N_2: *L(P)* for species I follows a Henry's Law isotherm with Henry's constant K_H and pressure *P*:

$$L(P) = K_H P$$

CO_2: *L(P)* for species I follows a Langmuir isotherm with saturation loading *M* and Brunauer-Emmett-Teller (BET) constant *K*:

$$L(P) = M\frac{K_A P}{(1 - K_B P)(1 - K_B P + K_A P)}$$

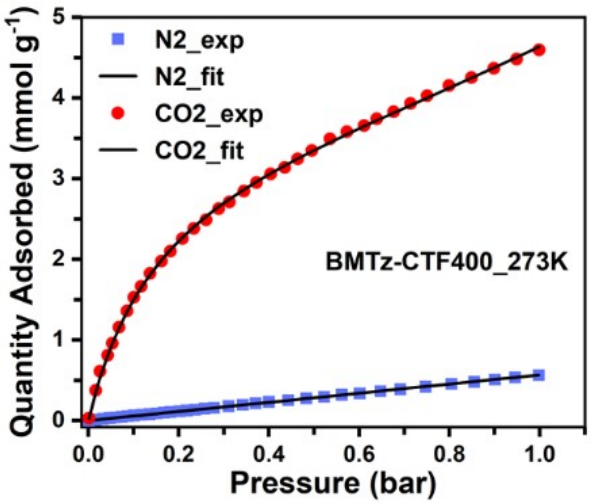

	K_H	M	K_A	K_B
CO_2		3.563924101	6.656265869	0.304300588
N_2	0.567274502303769			

Figure S9. IAST fitting for CO_2 and N_2 isotherm measured at 273 K in **BMTz-CTF600**.

N_2: *Li(P)* for species I follows a Henry's Law isotherm with Henry's constant K_H and pressure *P*:

$$Li(P) = K_H P$$

CO_2: *Li(P)* for species I follows a Langmuir isotherm with saturation loading *M* and Langmuir constant *Ki*:

$$Li(P) = M\frac{KiP}{1 + KiP}$$

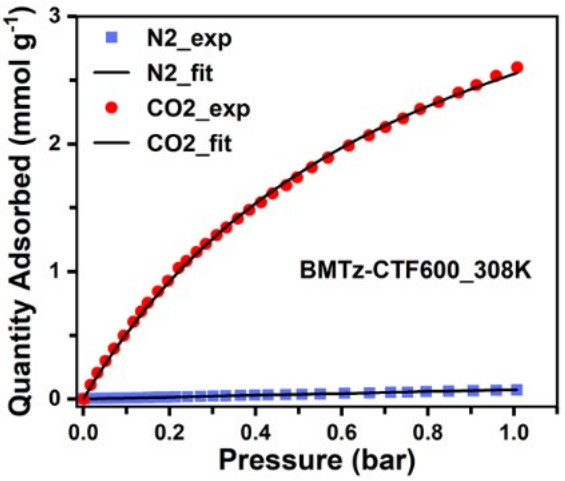

	K_H	M	Ki
CO_2		4.557701963	1.26943593
N_2	0.07431606644432334		

Figure S10. IAST fitting for CO_2 and N_2 isotherm measured at 308 K in **BMTz-CTF600**.

N_2: *Li(P)* for species I follows a Henry's Law isotherm with Henry's constant K_H and pressure *P*:

$$Li(P) = K_H P$$

CO_2: *Li(P)* for species I follows a Langmuir isotherm with saturation loading *M* and Dual-site Langmuir constant *K*:

$$Li(P) = M_1 \frac{K_1 P}{1 + K_1 P} + M_2 \frac{K_2 P}{1 + K_2 P}$$

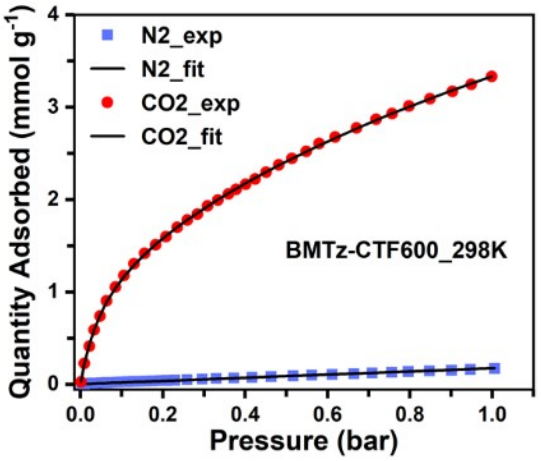

	K_H	$M1$	$K1$	$M2$	$K2$
CO_2		6.950840169	0.432413489	1.303598251	18.42116824

N_2	0.171908				

Figure S11. IAST fitting for CO_2 and N_2 isotherm measured at 298 K in BMTz-**CTF600**.

N_2: *L(P)* for species I follows a Henry's Law isotherm with Henry's constant K_H and pressure *P*:

$$L(P) = K_H P$$

CO_2: *L(P)* for species I follows a Langmuir isotherm with saturation loading *M* and Brunauer-Emmett-Teller (BET) constant *K*:

$$L(P) = M\frac{K_A P}{(1 - K_B P)(1 - K_B P + K_A P)}$$

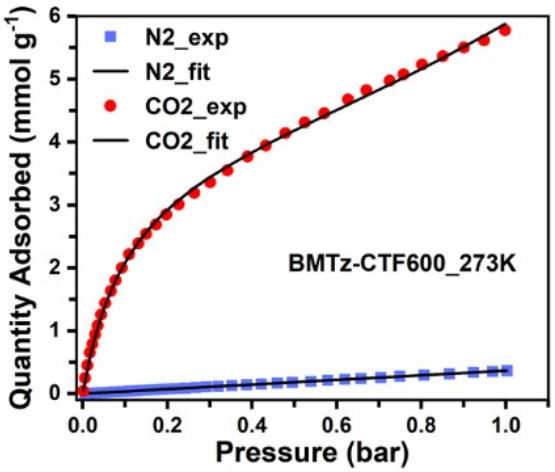

	K_H	M	K_A	K_B
CO_2		4.002189353	9.721862861	0.361740293
N_2	0.365572			

Figure S12. IAST fitting for CO_2 and N_2 isotherm measured at 273 K in **BMTz-CTF600**.

Section J. Electrochemical measurements:

The working electrode slurry was prepared by thoroughly mixing the BMTz-CTF400/600 (active material), Super P carbon black (conducting agent), and poly (vinylidene fluoride) (binder) at a weight ratio of 8:1:1 in N-methyl pyrrolidone (NMP)[65]. The as-prepared slurry was coated on a precleaned glassy carbon (GC) electrode followed by drying under a vacuum to get a modified GC as a working electrode. A three-electrode experimental setup was done using the modified GC as the working electrode, Ag/AgCl electrode as a reference, and a

platinum wire as a counter electrode in 1M H_2SO_4 to carry out electrochemical measurements of both BMTz-CTF400 and BMTz-CTF600 materials. All the electrochemical measurements were conducted with a **CHI7091E** electrochemical workstation. Cyclic voltammetry (CV) was carried out in the potential window of -0.1 V to 0.8 V under various scan rates ranging from 1 mV s^{-1} to 100 mV s^{-1}. At open circuit potential (OCP), the EIS measurements were carried out in the frequency range of 0.01 Hz to 100 kHz with an amplitude of 5 mV. The galvanostatic charge-discharge (GCD) measurements were executed at current densities from 0.5 A g^{-1} to 10 A g^{-1}. **Equation 1** was used for the calculation of gravimetric capacitance (C) from the GCD method in three-electrode assemblies [65]

$$C = \frac{I \times \Delta t}{m \times \Delta V} \qquad \textbf{(1)}$$

where I is the current (ampere) applied, Δt is the discharge time (second), ΔV is discharge voltage (volt) and m is the mass (g) of the active material (BMTz-CTFs).

Aqueous symmetric two-electrode supercapacitor device was fabricated for both BMTz-CTF400 and BMTz-CTF600 using a coin cell (CR2032). While doing so, a homogeneous slurry was prepared by grinding 80% Active material, 10% PVDF, 10% Super P Carbon black, and NMP in an agate mortar followed by coating on a circular graphite foil with a diameter of 14 mm and dried inside a vacuum oven at 80 ^oC for overnight. Mass loading was adjusted to 2.3-2.8 mg. Two electrodes (cathode and anode) were separated by using a separator (Whatman No 1 filter paper) pre-soaked into 1M H_2SO_4 and assembled into a coin-type cell. Furthermore, we designed a flexible symmetric supercapacitor to demonstrate the widespread practical utility of BMTz-CTF600 as both anode and cathode using a PVA-H_2SO_4-based gel electrolyte. For the fabrication of anode and cathode using electrode BMTz-CTF600 material, the same slurry preparation method was adopted as mentioned above and was coated over a carbon cloth (1 cm^2) and dried overnight inside a vacuum oven at 80 ^oC. The gel electrolyte was prepared by adding 1g of polyvinyl alcohol (Average Mw 89000-98000, Sigma-aldrich) in 10 ml of deionized water followed by stirring at 85 ^oC for 2 hours until the solution became clear. Then 1g of H_2SO_4 was dropwise added to it and stirred at room temperature for 1 hour.[85] The BMTz-CTF600 loaded carbon cloths were coated with the freshly as-prepared PVA/H_2SO_4 gel. Finally, the device was fabricated by sandwiching two similar electrodes via gentle heating, which was directly used for further electrochemical characterization.

Equation 2 was used for the calculation of gravimetric capacitance from the GCD method in two-electrode assembly.[72]

$$C = \frac{2 \times I \times \Delta t}{m \times \Delta V} \quad (2)$$

Equation 3 and **Equation 4** were used for the calculation of Energy density (Wh/kg) and power density (W/kg) for two-electrode assembly.[72]

$$E = \frac{C \times \Delta V^2 \times 1000}{2 \times 4 \times 3600} \quad (3)$$

$$P = \frac{E \times 3600}{\Delta t} \quad (4)$$

where I is the current (ampere) applied, Δt is the discharge time (second), ΔV is discharge voltage (volt) including IR drop and m is the mass (g) of the active material in one electrode, respectively.

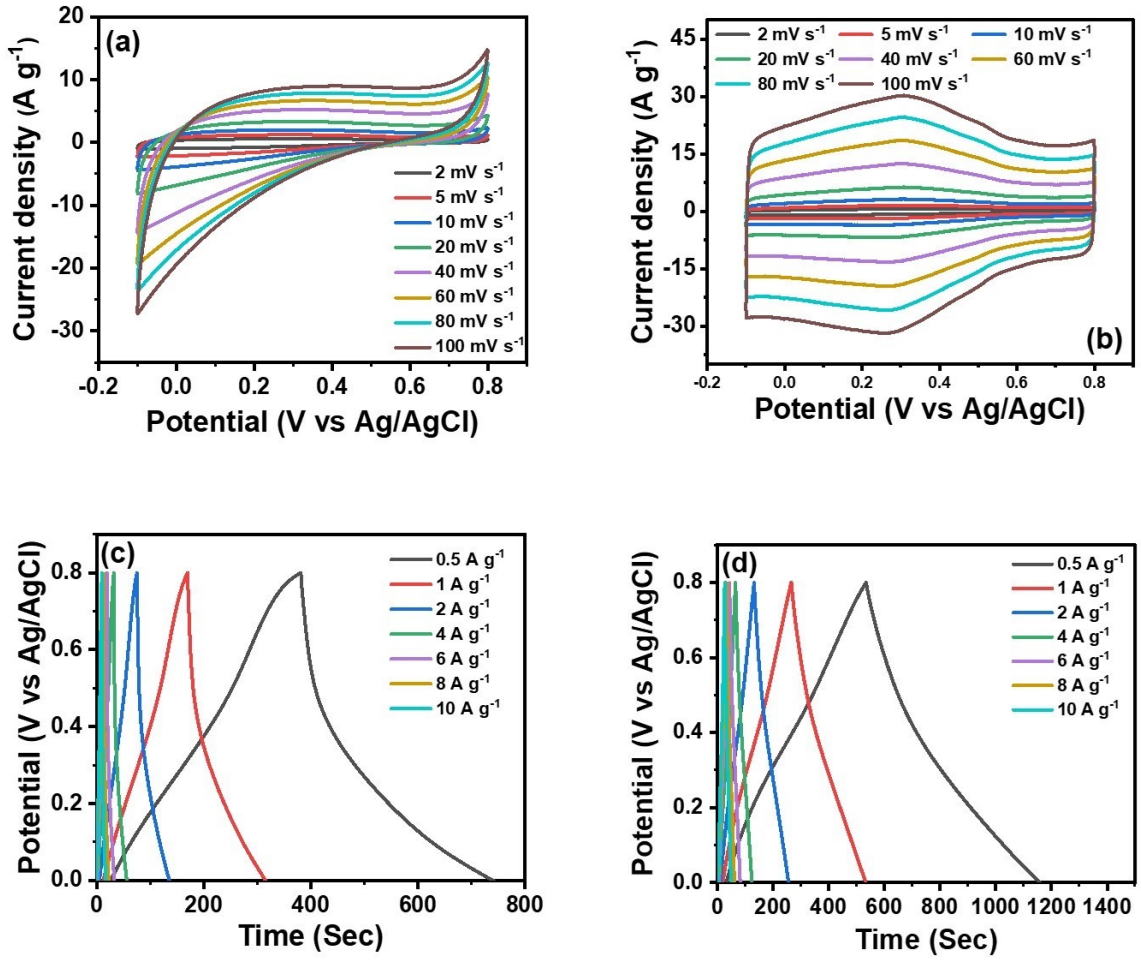

Figure S13: CV curves at different scan rates for (a) BMTz-CTF400, and (b) BMTz-CTF600. GCD curves at different current densities for (c) BMTz-CTF400, and (d) BMTz-CTF600.

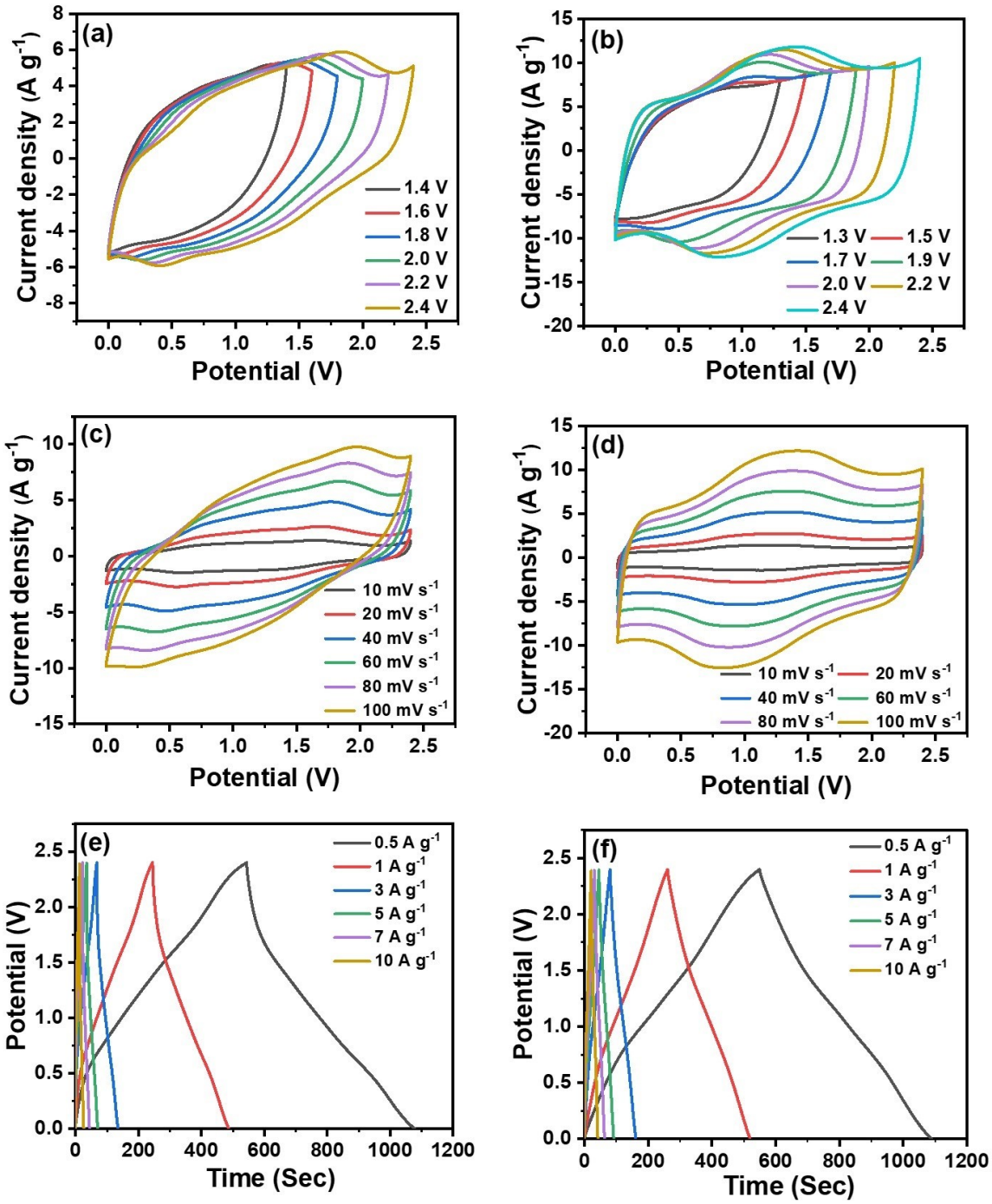

Figure S14: CV curves at different potential windows (a) BMTz-CTF400 (b) BMTz-CTF600, CV curves at different scan rates - (c) BMTz-CTF400 (d) BMTz-CTF600, and GCD at various current densities - (e) BMTz-CTF400 (f) BMTz-CTF 600.

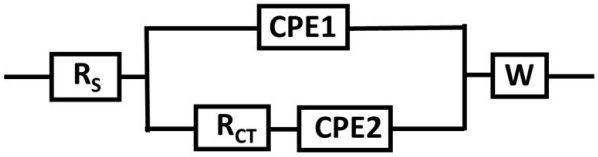

Figure S15: An equivalent circuit model for fitting the Nyquist plots for aqueous symmetric supercapacitor device of BMTz-CTF600.

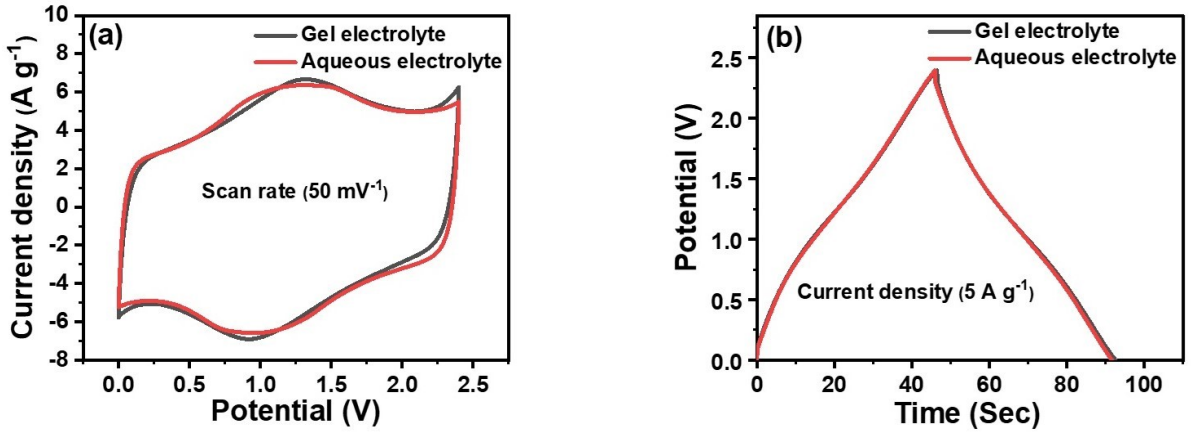

Figure S16: Comparison of electrochemical performance of aqueous vs gel electrolyte based two-electrode symmetric supercapacitor device made from BMTz-CTF600: (a) Comparison of CV curves at a scan rate of 50 mV s^{-1} (b) Comparison of GCD curves at a current density of 5 A g^{-1}.

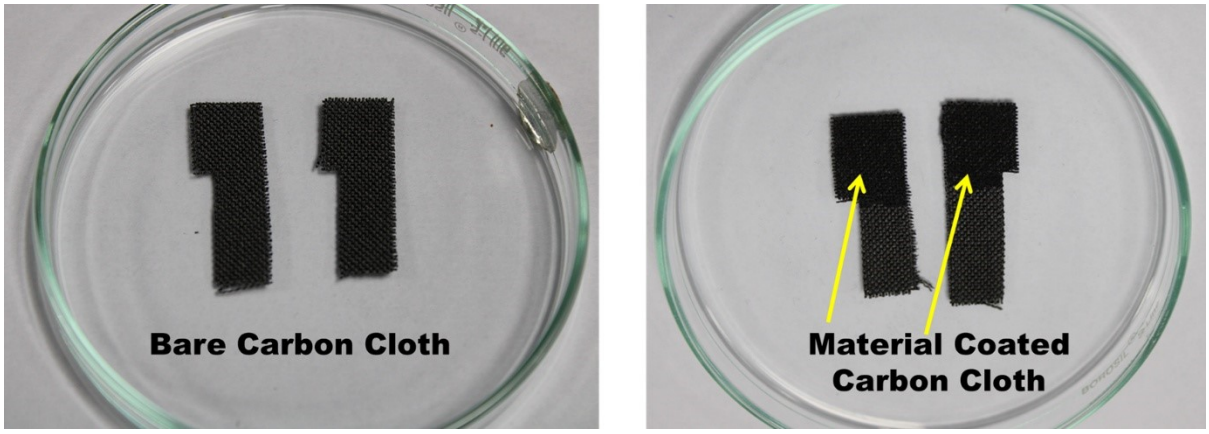

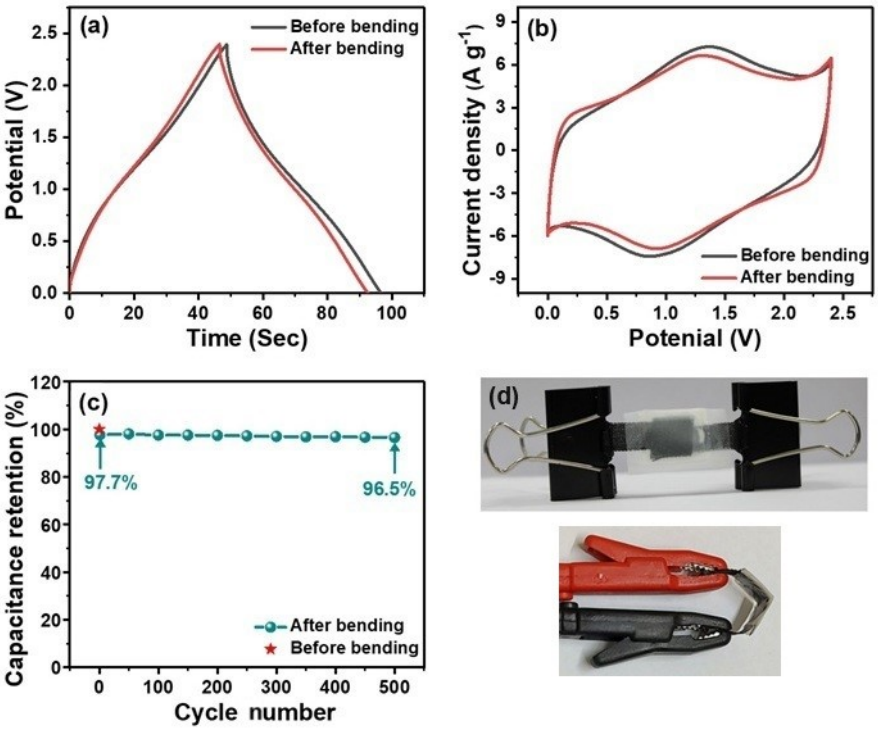

Figure S17: Comparison of electrochemical performances of flexible device before and after bending made from BMTz-CTF600: (a) Comparison of GCD curves at a current density of 5 A g^{-1}, (b) Comparison of CV curves at a scan rate of 50 mV s^{-1}, (c) Cyclic performance of flexible device after bending at 90 degree for 500 cycle at a current density of 5 A g^{-1}, and (d) As-prepared flexible device.

Section K: Comparison Tables:

Table S2. Comparison of the dual functionality of CTFs based POPs investigated in this work and other benchmark POPs for the two-electrode aqueous supercapacitor and CO_2 uptake performance in the literature.

Electrode Material	Specific capacitance[1]	Energy Density[2]	Power Density[3]	Cycle (Retention)	CO_2 Uptake[4]	IAST Selectivity[5]	Ref.
BMTz-CTF600	**225.7 (0.5)**	**44.7**	**298.7**	**20000@10 A g^{-1} (94.2%)**	**5.77 (2.54)**	**82**	**This Work**
BMTz-CTF400	**213.3 (0.5)**	**41.6**	**280.5**	**10000@10 A g^{-1} (88.4%)**	**4.60 (1.93)**	**57**	
poly(Cr-TPA-4BZ-Py-POP)-800	159.2 (1.0)	5.53	500	ND	4.4 / (ND)	ND	94
IITR-COF1	30.5 (0.12)	17.0	199.3	10000@1.2 A g^{-1} (111.3%)	2.29 / (ND)	ND	89
PAC-KOH	260 (1.0)	29.3	900	N.D.	6.57 / (ND)	ND	92
CF-800	~198 (0.5)	26.4	543.4	10000@3A g^{-1} (98%)	3.45 / (ND)	ND	S2
AC-TBG	45 (1.0)	ND	ND	15000@1 Ag^{-1} (ND)	4.5 / (ND)	ND	91
N,O-PC-CNT	176 (0.5)	5.3	500	20000@20 Ag^{-1} (95%)	5.7 / (ND)	ND	S3
A-NCs	102.1 (0.5)	20.4	299.7	2000@2 A g^{-1} (97.6%)	5.6 / (ND)	ND	S4
CPC-3	95 (0.5)	ND	ND	ND	5.3 / (ND)	ND	S5
PTCT-C	558 (1.0)	ND	ND	1000@2 A g^{-1} (95%)	4.63 (2.52)	ND	S6

[1]Two electrode specific capacitance in F g^{-1} and values in parenthesis in A g^{-1}. [2]Energy Density in Wh kg^{-1}. [3]Power Density in Wkg^{-1}. [4]Gas uptake in mmol g^{-1} at 1 bar and values in parenthesis in mmol g^{-1} at 0.1-0.15 bar at 273 K. [5]Calculated by IAST method at molar ratio of 15/85 for CO_2/N_2 at 298 K. ND: Not Determined

Table S3. The comparison of Supercapacitor performance of BMTz-CTF600 with recently reported Metal Free Porous carbon and related materials (symmetric two electrode device).

Electrode Material	**Electrolyte**	**Specific Capacitance ($F\ g^{-1}$) @ ($A\ g^{-1}$)**	**Potential Window**	**Energy Density (Wh/kg)**	**Power Density (W/kg)**	**Cycle**	**Retention /$A\ g^{-1}$**	**Refs.**
BMTz-CTF600	**1M H_2SO_4**	**225.7@0.5**	**2.4 V**	**44.7 → 32.1**	**298.7 → 5526.8**	**20000**	**94.2%/10**	**This Work**
IITR-COF1	0.5M K_2SO_4	30.5/0.12	2V	17	119.3	10000	111.3%/1	89
poly(Cr-TPA-4BZ-Py-POP)-800	1M KOH	159.2/1	0.5V	5.53	500	ND	ND	94
Polyaniline-Coated Mesoporous Carbon	PVA-H_2SO_4	107.8/0.5	0.8 V	9.59	200.1	1000	73.8 %/0.5	87
C–H_2O_2/HAc	3M KOH	ND	1.2V	23.33	ND	10000	98%/ND	S7
SNC	1M H_2SO_4	128/0.5	0.9 V	14.4	224.2	1000	95%/ND	88
PDA-FCC	1M PVA-H_2SO_4	61/1	1.2 V	11.7	385.3	10000	75%/5	90
N, S-HPCNSs	1M Na_2SO_4	61.8/0.2	1.8 V	27.8	180	10000	97.9 %/2	100
PAN/Konjac-800-1	PVA-KOH	258/0.5	1V	9	250.2	6000	90%/5	99
NP-HPCN-900-KOH	6M KOH	340/ 0.5	1.8 V	38.3	128.8	ND	ND	93
(CPCS)	6M KOH	70.92/0.5	1V	9.85	250	10000	100%/5	95
3D-NGF	6M KOH	242/1	1V	8.40	510	100000	77.6 %/4	96
MDPC-2	1M Na_2SO_4	67/0.5	2V	37.2	558	10000	98.1%/5	97
PPy-1.5	1M Na_2SO_4	62.5/0.5	1.4 V	ND	ND	10000	81.3 %/6	S8
NS-a-PCM-1000	6M KOH	ND	1V	17.3	250	23000	90%/10	98
HPCs-60	6M KOH	78.2/0.25	1 V	10.9	125	20000	89.9/10	S9
C-Phl	1M H_2SO_4	628/0.2 (3E)	1 V	ND	ND	ND	ND	S10

Table S4. Comparison of CO_2 uptake performance and IAST CO_2/N_2 IAST selectivity of BMTz-CTFs with other prominent POP-based adsorbents in the literature.

POP-based Adsorbents	CO_2 Uptake (mmol g^{-1})			Q_{st} (kJ mol^{-1})	IAST Selectivity*	References
	273 K (1 bar)	298 K (1 bar)	(0.1-0.2 bar)		298 K	
BMTz-CTF600	5.77	3.33	2.54 (273 K/0.15)	38	82	This Work
BMTz-CTF400	4.60	2.78	1.93 (273 K/0.15)	34	57	This Work
CQN-1e	6.58	4.39	ND	41.7	44.6	*Angew. Chem., Int. Ed.* **2019**, *58*, 872.
CQN-1g	7.16	4.57	1.03 (298 K/0.1)	40.6	42.7	
NRPP-1	6.1	2.22	ND	28	21	*ACS Appl. Mater. Interfaces* **2018**, *10*, 16049.
NRPP-2	7.06	3.71	ND	29.1	36	
ALP-1	5.37	3.25	ND	29.2	28	*Chem. Mater.* **2014**, *26*, 1385.
ALP-2	4.80	2.46	ND	27.9	26	
TBILP-2	5.59	3.32	0.92 (298 K/0.15)	29.0	43	*Macromolecules* **2014**, *47,* 8328.
Zn@AB-COF	4.68	1.79	ND	31.8	55	*Chem. Mater.* **2015**, *27*, 7874-7881
Li@AB-COF	4.33	1.43	ND	32.2	16	
SNU-C1-sca	4.38	3.14	ND	31.2	88	*Chem. Eur. J.* **2013**, *19*, 11590.
TSP-2	4.10	2.6	ND	30.8	25	*Chem. Commun.* **2014**, *50*, 7933.
bipy-CTF500	5.34	3.07	ND	34.2	42	20
bipy-CTF600	5.58	2.95	ND	34.4	24	
lut-CTF350	4.06	2.41	ND	37.4	66	
lut-CTF400	4.55	2.72	ND	37.5	53	
lut-CTF500	5.04	2.58	ND	38.2	27	
lut-CTF600	4.99	2.52	ND	33.3	23	
fl-CTF-350	4.28	2.29	ND	32.7	23	*J. Mater. Chem. A* **2014**, *2*, 5928.
fl-CTF-400	4.13	1.97	ND	30.7	16	
FCTF-1	4.67	3.21	0.92 (298 K/0.1)	35	31	*Energy Environ. Sci.,* **2013**, *6*, 3684
LKK-CMP-1	2.22	1.38	ND	35.0	44.2	*Ind. Eng. Chem. Res.* **2018**, *57*, 9254.
COF@PEI	2.18		ND	21.8	17.6	*J. Mater. Chem. A,* **2019**, *7*, 4549
[AeImBr]83% -TAPT-COF	ND	2.67	ND		45.3	*ACS Appl. Mater. Interfaces* **2022**, *14,* 55674.
TOK-700	5.76	3.61	2.81 (273 K/0.2)	37.8	65	*Carbon* **2021**, *172*, 71.
Pz-CTF6	4.19	2.47	ND	37.3	147	*Chem. Eng. J.* **2022**, *429*, 132160.
[HO_2C] 100 % -H_2 P-COF	3.95	1.72	ND	43.5	77	*Angew. Chem. Int. Ed.* **2015**, *54*, 2986.

*CO_2/N_2 (15:85)

Section L: References:

S1. W. Lu, Z. Wei, D. Yuan, J. Tian, S. Fordham and H.C. Zhou, *Chem. Mater.,* 2014, **26**, 4589.

S2. V. Hiremath, A. C. Lim, G. Nagaraju and J. G. Seo, *ACS Sustainable Chem. Eng.,* 2019, **7**, 11944.

S3. J. Hao, X. Wang, Y. Wang, X. Lai, Q. Guo, J. Zhao, Y. Yang and Y. Li, *Nanoscale Adv.,* 2020, **2**, 878.
S4. H. Wei, H. Chen, N. Fu, J. Chen, G. Lan, W. Qian, Y. Liu, H. Lin and S. Han, *Electrochim. Acta.,* 2017, **231**, 403.
S5. G. Singh, R. Bahadur, A. M. Ruban, J. M. Davidraj, D. Su and A. Vinu, *Green Chemistry.,* 2021, **23**, 5571.
S6. H. Wang, Z. Cheng, Y. Liao, J. Li, J. Weber, A. Thomas and C. F. J. Faul, *Chem. Mater.,* 2017, **29**, 4885.
S7. S. Y. Lu, M. Jin, Y. Zhang, Y. B. Niu, J. C. Gao and C. M. Li, *Adv. Energy Mater.,* 2017, **8**. 1702545.
S8. T. Wang, Y. Wang, D. Zhang, X. Hu, L. Zhang, C. Zhao, Y. S. He, W. Zhang, N. Yang and Z. F. Ma, *ACS Appl. Mater. Interfaces,* 2021, **13**, 17726.
S9. Y. Yang, D. Chen, W. Han, Y. Cheng, B. Sun, C. Hou, G. Zhao, D. Liu, G. Chen, J. Han and X. Zhang, *Carbon,* 2023, **205**, 1.
S10. T. Wang, R. Pan, M. L. Martins, J. Cui, Z. Huang, B. P. Thapaliya, C.-L. Do-Thanh, M. Zhou, J. Fan, Z. Yang, M. Chi, T. Kobayashi, J. Wu, E. Mamontov and S. Dai, *Nat. Commun.,* 2023, **14**, 4607.